Available online at www.sciencedirect.com

SciVerse ScienceDirect

Journal of the European Ceramic Society 32 (2012) 2219–2233

www.elsevier.com/locate/jeurceramsoc

Corrosion of ceramics for vinasse gasification in supercritical water

Thierry Richard [a,*], Jacques Poirier [a], Cedric Reverte [b], Cyril Aymonier [b], Anne Loppinet-Serani [b], Gökalp Iskender [c], Escot-Bocanegra Pablo [c], Frederic Marias [d]

[a] CEMHTI - Conditions Extrêmes et Matériaux: Haute Température et Irradiations, CNRS, Université d'Orléans, 1b avenue de la recherche scientifique, 45071 Orléans, cedex, Orléans, France

[b] ICMCB, Institut de Chimie et de la Matière Condensée de Bordeaux, Université de Bordeaux, CNRS, 87 avenue du Dr. A. Schweitzer, Pessac F-33608, France

[c] ICARE, Institut de Combustion, Aérothermique, Réactivité et Environnement, CNRS, 1c avenue de la recherche scientifique, 45071 Orléans, France

[d] LATEP, Laboratoire de Thermique, Energétique et Procédés, Rue Jules Ferry, 64000 Pau, France

Received 14 September 2011; received in revised form 17 February 2012; accepted 2 March 2012
Available online 5 April 2012

Abstract

Supercritical water gasification (SCWG) is a very efficient process to convert wet biomass into energetic gases. Unfortunately, SCWG reactor may strongly corrode due to the addition of temperature, pressure and the presence of corrosive species. In the present paper, the corrosion of various ceramic materials in subcritical and supercritical water (SCW) gasification process was studied in a batch reactor. We compare the corrosion in distillated water and the corrosion in sugar beet slurry that will be gasified under supercritical conditions. The experimental temperatures were 350 °C and 550 °C and the pressure was 25 MPa. Technical ceramics (SiC, alumina, Y stabilized zirconia, Si_3N_4, BN, aluminosilicate, cordierite-mullite) show poor capability to sustain corrosion whereas graphite and glassy carbon are the highest performance materials in our working conditions.

Keywords: Corrosion; Supercritical water gasification; Ceramics; Wastewater

1. Introduction

Supercritical water (critical point: $T_c = 374\,°C$ and $P_c = 22.1$ MPa) is a favourable medium for chemistry applications. It has current applications in the field of bioenergy, organics destruction or material synthesis.[1–3] Supercritical water biomass gasification (SCBG) is an innovative and efficient way to convert humid biomass into a gas with a great heating value ($CO + H_2$ and/or methane).[1] Contrary to supercritical water oxidation process (SCWO), supercritical water gasification process (SCWG) operates in a very poor oxygen environment. In these conditions, organic matter decomposes mainly into H_2, CH_4, CO, and CO_2 under the effects of both pyrolysis and hydrolysis reactions.[4,5] Regarding the temperature these reactions can also lead to numerous organic molecules recovered at the end of the process in the liquid phase.[6] The reactions involved are quite complex even in the case of simple and well-known organic molecules like glycerol, glucose or formic acid.[5,7,8]

This SCWG process has many economic and environmental advantages:

(1) biomass can be converted without drying, which would be prohibitive for the overall energy balance;
(2) in supercritical water, most of the organic compounds become soluble;
(3) the overall reaction kinetics are very efficient due to the high diffusivity in supercritical mixtures and generally homogeneous reaction medium;
(4) compared to "classical gasification", SCWG is a low temperature process so no polycyclic aromatic hydrocarbons, no NOx and no SOx are produced;
(5) the produced gas is hydrogen rich.

The SCBG process can combine the action of pressure and temperature in complex fluids containing corrosive species (for instance chlorides and alkali) in different concentrations. Material corrosion is a challenge in SCWG due to the feedstock

* Corresponding author. Tel.: +33 238 256 688; fax: +33 238 638 103.
E-mail address: thierry.richard@cnrs-orleans.fr (T. Richard).

0955-2219/$ – see front matter © 2012 Elsevier Ltd. All rights reserved.
doi:10.1016/j.jeurceramsoc.2012.03.007

variability. The use of metal and alloys to build gasification reactors is limited for three main reasons:

(1) The creep at quite elevated pressure (30 MPa) limits the working temperature around 600 °C. Over this limit the mechanical strength decreases and materials do not sustain pressure anymore. Actually, the creep resistance depends on the alloys mechanical properties and on 3 external parameters: temperature, pressure and time. For creep resistance, there is an equivalency between the time and the temperature. At a given pressure, if the temperature increases then the rupture life decreases. At the opposite if we want to increase the rupture lifetime we have to reduce the temperature conditions. Commercial reactors must be designed for a long time of utilization (100,000 h) it defines the temperature and pressure limit.
(2) Material grade must also be chosen with care because some type of alloy cannot sustain every corrosive condition.[9]
(3) As outlined by Kruse,[10] hydrogen is known to be able to change the mechanical stability of metals. Direct interaction between H_2 and materials cannot be excluded and the action of a highly concentrated H_2 atmosphere may be destructive for metals.

Corrosion is known to be more severe in near-critical water than in supercritical water. In this near-critical region water density, ionic product and temperature are high enough to influence chemical reactions.[9] However, significant corrosion may occur in supercritical conditions even if ionic reactions are not supported. Solid salt deposits can create a local corrosive environment where water or brine can be trapped between the solid layer and the wall. At higher temperature, molten salt can also be corrosive. Material corrosion is a serious issue in supercritical water processes because strongly oxidizing (SCWO) or more reducing (SCWG) conditions can be created.[11]

Many studies are devoted to metallic or alloys corrosion in SCW. Most of them are parametric studies of corrosion in SCWO conditions, in the presence of oxygen, acids and salts.[12–16] Nickel-based alloys are preferred for such applications because of their chemical and mechanical stress resistance at both elevated temperature (from ambient up to 600 °C) and pressure (30 MPa). Hwang et al.[17] outlined the highest performance of Ni alloys compared to Ferritic/Martensitic steel in deionized supercritical water. Anyway, corrosion is dependent upon environmental factors (density, temperature, pH, electrochemical potential, presence of anions and heat treatments) and on material characteristics (alloy composition, purity, surface properties).[9] The corrosion resistance of metals and alloys can be explained by passive oxide film formation on their surfaces. In supercritical water gasification condition, oxide film stability may be limited by the formation of reductive gas (H_2, CH_4). In low electrochemical potentials, active dissolution of many metals (Fe, Ni, Cr, etc.) may occur.[11] D'Jesus et al.[18] observed the reduction of a NiO passivating film formed on the surface of 625 nickel alloy at only a few bars of hydrogen partial pressure although thermodynamical calculation shows that it should happen at higher partial pressure (10 MPa). The specificity of SCWG and the different types of corrosion encountered are outlined by Marrone and Hong.[11] Kruse[10] reports that nickel-based alloy 625 was used for more than 1000 h in SCWG experiments with methanol and that hydrogen formation does not seem to be problematic for gasification reactor under these experimental conditions. Sometimes corrosion was found due to the presence of sulfur or K_2CO_3 in the reacting media.[10] On the other hand, a significant corrosion of nickel-based alloys (including Inconel® 625 and Hastelloy C276) had been reported by Calzavara et al.[19] Obviously, there is no universal material that could withstand all types of biomass in every set of operating conditions.

Ceramics are very resistant under extreme conditions and may be considered as material to build an anticorrosive wall for biomass gasification reactors. Few papers are devoted to ceramic behavior in hydrothermal environments. As hydrothermal oxidation is very efficient to treat hazardous compounds, dioxins, and to destroy halogenated species,[20] ceramic corrosion has been studied for the supercritical water oxidation process in the presence of acidic or chlorinated species. Boukis et al.[21] show a screening test of high performance ceramics in supercritical water containing oxygen and hydrochloric acid. In this paper 33 ceramics have been studied. Other papers devoted to the corrosion of technical ceramics like SiC,[22,23] Si_3N_4,[21] alumina,[24] zirconium oxides[25] can be found in the literature. All of them deal with specific conditions related to SCWO. Unfortunately, all results obtained in an oxidative environment may be of poor interest in the case of reductive conditions.[11] To our knowledge, there are only a few papers dealing with material corrosion in SCWG and none that discusses the specific use of ceramics.[11]

The aim of this paper is to study the corrosion behavior of various ceramic materials and carbon (graphite and glassy carbon) materials in subcritical and supercritical water biomass gasification in a batch reactor. The real biomass used in this study is sugar beet slurry also called "vinasse".

2. Experimental

2.1. Materials

The fluid used is either distillated water or sugar beet slurry called "vinasse". The high water content and the high organic concentration make this resource reliable for the supercritical water biomass gasification (SCBG) treatment. The global composition of this slurry is given in Table 1. A quantitative analysis of atomic species has been performed by ICP-OES (720ES – Varian Company). Anions have been characterized by liquid chromatography using the Dionex DX-120 chromatograph with ion pac AS14A and AG14A column. The eluent was a mix of $NaHCO_3$ and Na_2CO_3. The results are presented in Table 2.

During the supercritical water treatment, organic materials from biomass are converted into gas, liquid and solid phase whose balance depends especially on temperature. The composition of the liquid phase (water soluble and insoluble species) in such converted biomass with SCBG is generally complex as reported elsewhere by Carrier et al.[6] The gas contains reductive species (like H_2 or CH_4) and forms a reactive atmosphere that may lead to materials corrosion. In gasification the

Table 1
Concentrated vinasse composition.

Bio-resource	Water content (wt.%)[a]	Mineral elements in the sample (wt.%)[b] (w.b)[c]	Elementary analysis (wt.%) (w.b.)[c]				HHV[e] (MJ kg^{-1}) (d.b.)[f]	LHV[e] (MJ kg^{-1}) (d.b.)[f]
			C	H	N	O[d]		
Concentrated "vinasse"	48.3	9.0	23.3	8.1	3.8	55.8	15.7	14.6

Source: ICMCB.
[a] Water content = 100% − dry matter content.
[b] Determined by ICP-OES.
[c] On a wet basis.
[d] By difference (O% = 100% − mineral elements% − C% − H% − N%).
[e] Higher heating value (HHV) and lower heating value (LHV).
[f] On a dry basis.

Table 2
Anionic concentration by liquid chromatography (Dionex DX 120) and cationic concentration by ICP-OES. Results are given in mg l^{-1}.

	pH	Conductivity (mS cm^{-1})	Cl^-	NO_3^-	PO_4^{3-}	SO_4^{2-}	K^+	Na^+	P^{3+}	Ca^{2+}	Others[a]
Concentrated vinasse	6.07	15.08	5653	137	450	3686	32	10	1.3	1.2	0.5

[a] Al, As, Ba, Cr, Fe, Mg, Si, Zn.

Table 3
Gas yield as a function of temperature (wt.%).

	Yield (wt.%)		
	400 °C	450 °C	500 °C
Concentrated vinasse			
Gas phase	3.6	4.3	4.7
Aqueous phase	49.9	56.2	54.7
Organic liquid phase	39.4	30.3	33.5
Organic solid phase	3.5	2.4	2.9

presence of H_2, CO, CH_4 and water can cause an attack of the oxide protective film formed on the surface of the alloys, or H_2 embrittlement may lead to the fast propagation of cracks in the reactor. The gas composition is then as important as the mineral content for the corrosion study and was obtained by gas chromatography (Fig. 1). Gas Chromatography is carried out with a Varian micro-GC CP-4900 with TCD detector (analyzed gases: H_2, CO, CH_4, CO, N_2). The second instrument used is a gas chromatography Varian (GC-3600) for the analysis of CO_2 and light hydrocarbons if necessary. TCD and FID detectors

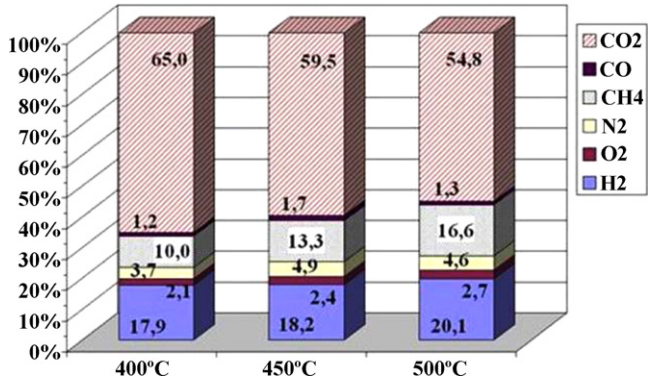

Fig. 1. Molar composition of the gas phase as a function of temperature. Measurements are made at ambient temperature and at atmospheric pressure.

are used. A capillary column is connected to FID (Carbowax for light hydrocarbons). Two columns are connected and are on-line to TCD (a column Porapaq for the separation of CO_2 from the other gases, and a molecular sieve). A system of valves separates CO_2 from the molecular sieve. Batch study shows that it is modified as temperature increases leading to high hydrogen content. The overall gas yield also increases with temperature (Table 3). For each experiment a small residual air fraction remains in the reactor as it is loaded with the aqueous waste (batch reactor), which explains the presence of O_2 and N_2 in the gas composition (Fig. 1).

Metallic based alloys are commonly used to build supercritical water oxidation or gasification reactors. Our batch reactor is made of Inconel® 718 so a careful observation of its corrosion behavior was made. We also used a standard stainless steel 316 L as a reference to compare with the ceramic corrosion. The chosen materials are solid bulk ceramics commonly used in industrial applications and they are known to be resistant under high temperature conditions. They belong to the well-known ceramic family like oxide, nitride, boride, and silica-based materials. SiC and alumina have been chosen for their good chemical stability in supercritical conditions. SiC is used in commercial nuclear reactors and shows a low corrosion rate in supercritical water at 500 °C.[22] Alumina has been used as a protective wall in supercritical water oxidation.[26] In spite of their thermal and

Table 4
Tested materials characteristics.

Bulk materials	Supplier	Trade name	Chemical purity (wt.%)	Hg-porosity	Bulk density ($\times 10^3$ kg m^{-3})	Mineralogy	R_a (μm)	R_t (μm)
Alumina	Anderman ceramiques	EA999 C-799	Al_2O_3 (99.99%)	0.0 ± 0.1%	3.8–3.95	α-Alumina	0.81	7.58
Graphite F	Final materials	R7340	C (99.98%)	18.4 ± 0.1%	1.72	2H	4.50	55.26
Graphite CL	Mersen	2020 PT	C (99.98%)	18.4 ± 0.1%	1.77	2H	3.35	24.41
Graphite L	Available at laboratory		C (>99.9%)	32.8 ± 0.1%	2.07	2H	3.82	33.32
Glassy carbon[a]	Mersen	V25	C (99.96%)	0.0 ± 0.1%	1.50–1.55	Vitreous	0.25 0.27	2.31 9.75
SiC 100	Available at laboratory		SiC	16.7 ± 0.1%	2.7	Moissanite 6H	13.80	102.95
SiC	Final materials	SIC 2500	SiC (99–99.5%)	0.0 ± 0.1%	3.1–3.2	Moissanite 6H	0.398	3.04
Graphite np	Mersen	H1H2	C (>99.9%)	0.5 ± 0.1%	1.64	2H	3.61	23.95
Stainless steel	Available at laboratory	316 L		0.0 ± 0.1%	8.0		1.66	9.73
Silicon nitride	Final materials	SIN1300	Si_3N_4 (>98%)	39.0 ± 0.1%	3.2–3.22	Hexagonal		
Boron nitride	Final materials	NB HD	BN (>98.5%)	2.4 ± 0.1%	2.2	Hexagonal	0.29	2.15
Y stabilized zirconia	Final materials	ZR1500	ZrO_2–Y_2O_3 (>99%)	1.5 ± 0.1%	5.5–5.8	ZrO_2 monoclinic $(ZrO_2)_{0.96}(Y_2O_3)_{0.04}$ tetragonal	1.47	12.15
Cordierite-mullite	Imerys Kiln Furniture	C1E	Al_2O_3 (40%), SiO_2 (49%), MgO (6.3%)	18.7 ± 0.1%	2.24	Orthorhombic	6.01	42.35
Aluminosilicate[b]	Available at laboratory		82% Al_2O_3	13.7 ± 0.1%	3.45	Mullite orthorhombic Al_2TiO_5 orthorhombic TiO_2 tetragonal Al_2SiO_5 orthorhombic Al_2O_3 rhombohedral	2.48	27.09

[a] Glassy carbon has 2 different surfaces states due to its fabrication process. We measured roughness for each surfaces.
[b] Refractory composite containing mullite, aluminum titanium oxide (Al_2TiO_5), titanium oxide (TiO_2), andalousite (Al_2SiO_5) and alumina.

chemical properties, non-oxide ceramics (SiC, BN, Si_3N_4) can show instability in the presence of an oxidant.[27] It is interesting to test the behavior of these ceramics in the presence of a reductive gas. In these reductive conditions carbon materials could be very efficient against corrosion. For instance diamonds are used in H-DAC (hydrothermal anvil cell) for in situ characterization of biomass gasification in supercritical water.[28] The samples are in the order of a few cm^3. The tested material characteristics are presented in Table 4.

Prior to the attack, the material porosity has been characterized by a micromeritics autopore IV Hg-porosimeter. The crystalline phases have been determined by room-temperature X-ray diffraction measurements carried out with a Bruker AXS D8 diffractometer (advanced diffractometer with a conventional *y–y* Bragg–Brentano configuration) fitted out with a Vantec 1 linear detector. For example and to help reproducibility surface roughness measurement has been made with a portative SM4 device. Calibration was made with a SM1441 standard with $R_a = 2.97\ \mu m$.

The corrosion resistance of several commercial ceramic materials was determined by weight loss measurements. An Olympus BX51 optical microscope with a Sony xcd U100CR CCD camera and a Hitachi S4500 (SEM-FEG) with an energy dispersive spectroscopy (EDS) system: OXFORD: ISIS 300 with a Si (Li) detector were also used for material characterization and corrosion study.

2.2. Methods

A first material selection was performed with short corrosion tests. They were performed in a 110 ml Inconel® 625 nickel base alloy in the presence of effluents with poor organic content (5 wt.%). This product comes from vinasse of methanization. The pressure was 25 MPa, the heating rate was 10 °C min^{-1} and the cooling rate was not regulated and could last up to 3 h to reach ambient conditions. The aim was to give first insights on the kinetics of corrosion of ceramics in hydrothermal conditions. In addition, as we started with a collection of very different materials, these preliminary tests were useful to separate stable ceramics from the others. Tests were carried out for a period of time between 10 and 20 h. Disintegrated and strongly corroded materials were analyzed and removed from the sample list.

All other corrosion tests have been performed in a 300 ml batch reactor (Fig. 2) made of nickel base alloy (Inconel® 718) in both deionized water and concentrated vinasse. Experiments lasted an average time of 300 h (∼12 days) but can last up to 870 h (∼36 days). Corrosion tests request long experimental periods, each run was performed with all the samples simultaneously. In this condition, mutual effects of the solubility of one sample to another is possible but it does not affect significantly the experiment for two reasons: (1) after the first material selection the sample have a low solubility, (2) The comparison is made between corrosion in supercritical water with and without the presence of biomass. All other parameters remain constant including the number and the nature of samples.

Experiments were performed in order to measure mass losses and to study the evolution of surfaces over time. The sample area

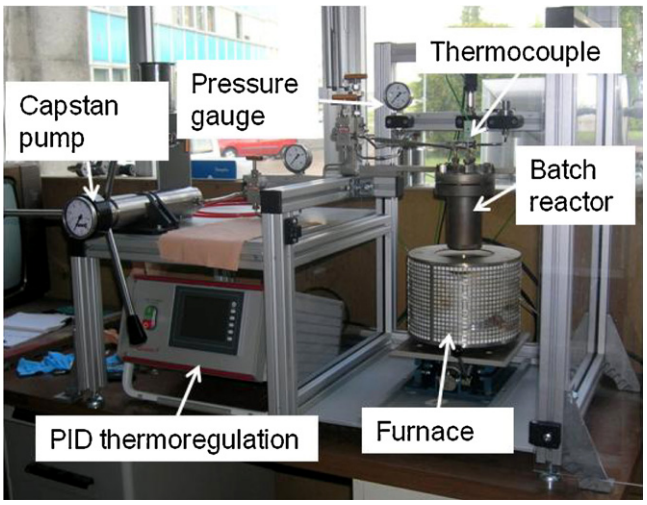

Fig. 2. 300 ml high pressure and high temperature batch reactor. $T_{max} = 550\ °C$, $P_{max} = 30.0$ MPa.

is determined by mechanical measurement and is supposed to be constant all along the experiment. This assumption is justified by the low solubility of the ceramics. A second assumption is that the corrosion takes place on the outer surface of sample. Then we define a mass variation by unit surface: d*G*/*A* (Tables 5–7).

The system is heated with an external furnace controlled by a PID controller device that controls the heating rate (10 °C min^{-1}) in order to stabilize the temperature with a good accuracy of ±5 °C at 550 °C. The experimental pressure is about 25 MPa. *P* and *T* are automatically recorded during the experiments, and are recorded every 5 s.

3. Results

A compilation of all corrosion tests is given in Tables 5 and 6. Weight change as a function of time spent in the corrosive environments is also reported in Fig. 3a–d. Only results from long time experiments in deionized water and concentrated vinasse are presented in these figures.

3.1. Preliminary corrosion tests

First screening tests were made with a wide selection of ceramics in supercritical water in the presence of the effluent (Table 5). Some observations made by Boukis et al.[21] are confirmed here in similar temperature and pressure conditions but in different environments (no acid, no additional O_2).

SiO_2 based materials (aluminosilicate, cordierite-mullite) are strongly corroded. We observed the formation of porosity and a deep penetration of the fluid. The deposition of potassium based solid in the porosity explains the huge mass gain for cordierite-mullite (Table 5). For the aluminosilicate, the potassium oxide deposition cannot compensate the dissolution of material.

Si_3N_4 and BN were strongly corroded in the supercritical environment. The BN was disintegrated. On the surface of Si_3N_4 sample, a thick porous layer is formed even at 400 °C.

Table 5
Weight change of ceramic materials tested in hot compressed effluent.

Bulk materials	Exposure time (h)	Weight change, dG/A ($\times 10^{-2}$ mg cm^{-2})			Comments
		Subcritical conditions	Supercritical conditions		
		350 °C; 25.0 MPa	400 °C; 25.0 MPa	550 °C; 25.0 MPa	
SiC 100	12	+450 ± 6			[b]
Glassy carbon	12	−2 ± 2			
316 L	12	−22 ± 3			
Aluminosilicate	12	−880 ± 7			Strong dissolution
Si_3N_4	23		+6484 ± 36		[b] Formation of a thick porous layer
Cordierite-mullite	23		+1874 ± 11		[b] solid deposition in porosities
SiC 100	23		+256 ± 4		[b]
Glassy carbon	23		+8 ± 2		
Aluminosilicate	23		−397 ± 21		
316 L	23		−21 ± 3		
BN	<8		Disintegrated		
Si_3N_4	14			+1219 ± 308	[b]
Cordierite-mullite	14			+1376 ± 347	[b]
SiC 100	14			+389 ± 35	[b]
Graphite L	14			+251 ± 10	[b]
316 L	14			+135 ± 6	[b]
Alumina	14			+81 ± 2	[b]
Glassy carbon	14			+0.6 ± 0.7	[b]
Aluminosilicate[a]	14			−504 ± 128	

[a] Samples have also been exposed to subcritical fluid for 10 h during the experiment.
[b] Positive mass are due to solid deposition on the materials surfaces that compensates the mass loss due to materials corrosion when it occurs. Salt formations are important in the supercritical water conditions.

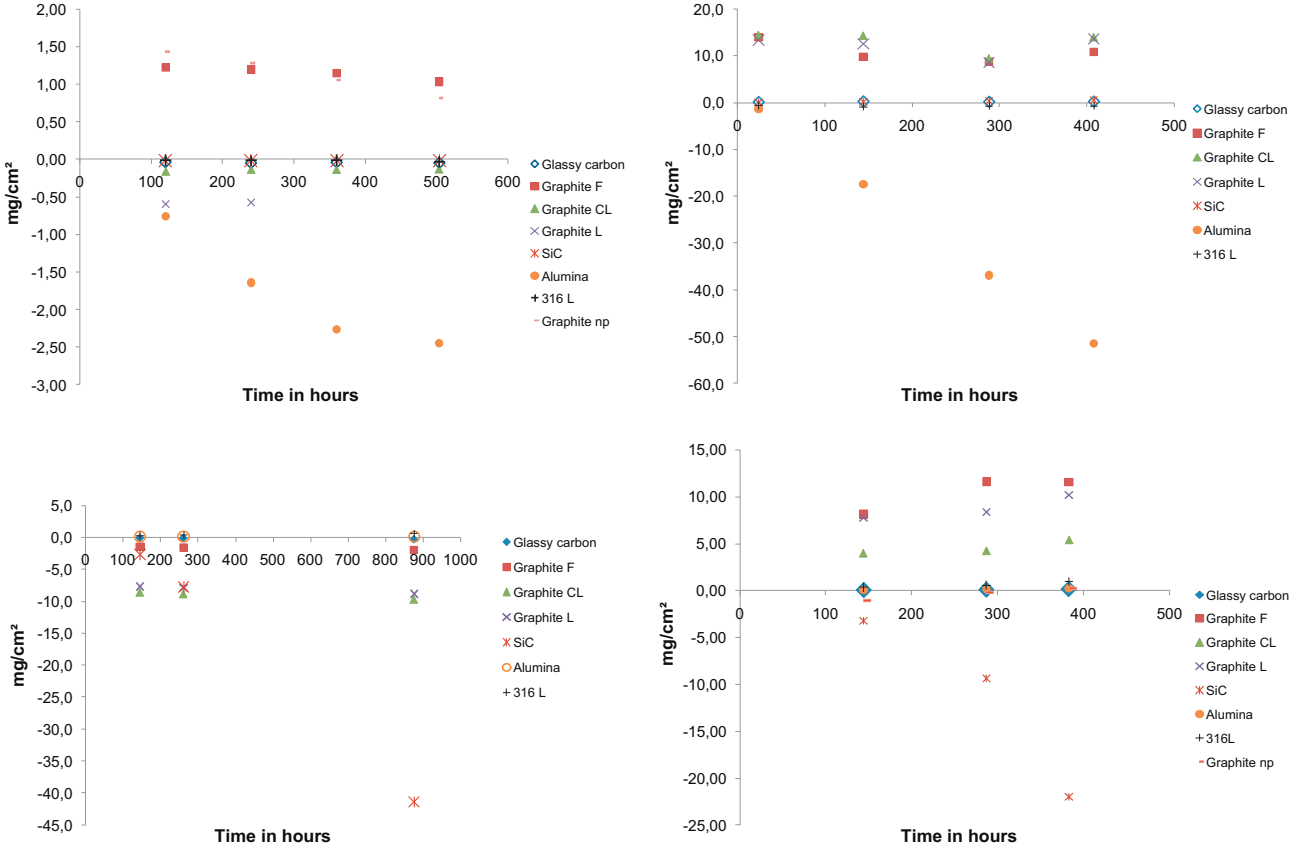

Fig. 3. (a) Weight change as a function of time exposure in subcritical deionized water at 335 °C and 21.5 MPa. (b) Weight change as a function of time exposure in supercritical deionized water at 550 °C and 25.0 MPa. (c) Weight change as a function of time exposure in subcritical water in the presence of vinasse at 350 °C and 25.0 MPa. (d) Weight variation as a function of time exposure in supercritical water in the presence of vinasse at 550 °C and 25.0 MPa.

Table 6
Weight change of ceramic materials tested in hot compressed distilled water.

Bulk materials	Exposure time (h)	Weight change, dG/A ($\times 10^{-2}$ mg cm^{-2})		Comments
		Subcritical conditions 335 °C; 21.5 MPa	Supercritical conditions 550 °C; 25.0 MPa	
Graphite F	504	+103 ± 25		Probably water penetration into small pores
Graphite np	504	+82 ± 7		Probably water penetration into small pores
SiC	504	−2 ± 3		No corrosion observed
Stainless steel	504	−3 ± 3		Localized pitting corrosion
Glassy carbon	504	−5 ± 2		No corrosion observed
Graphite CL	504	−13 ± 4		No corrosion observed
SiC 100	290	−21 ± 6		No corrosion observed
Graphite L[a]	240	−58 ± 5		
Alumina	504	−245 ± 30		Intergranular corrosion
Stainless steel	876		+62 ± 6	Formation of an oxide surface layer. Slight surface peeling
Alumina	876		+15 ± 3	Slight intergranular corrosion
Glassy carbon	876		−25 ± 4	No corrosion observed
Graphite F	876		−194 ± 2	[b]
Graphite L	876		−882 ± 31	[b]
Graphite CL	876		−968.3 ± 41	[b]
SiC 100	876		−1839 ± 114	Dissolution
SiC	876		−4143 ± 387	Dissolution

[a] A small piece of the material was broken.
[b] Mass loss invariant with time exposure due to specific sites (defects) oxidation.

Corundum, SiC and carbon materials are resistant in these conditions, but a longer time is necessary to study more precisely their corrosion resistance.

Thanks to these tests, "better" materials were chosen and observed with more accuracy. The tests lasted few hundred of hours in both pure deionized water and in vinasse under subcritical and supercritical conditions. Results are presented in the following section.

3.2. Long time corrosion tests

3.2.1. Metallic alloys

Nickel-based alloys are used to build supercritical water reactors instead of stainless steel because they can work at higher temperature under pressure. In addition, they are supposed to be more chemically resistant to corrosion in SCWO process. Their corrosion in SCW has been well studied and referenced by

Table 7
Weight change of ceramic materials tested in hot compressed water in the presence of concentrated vinasse.

Bulk materials	Exposure time (h)	Weight change, dG/A ($\times 10^{-2}$ mg cm^{-2})		Comments
		Subcritical conditions 330 °C; 25.0 MPa	Supercritical conditions 550 °C; 25.0 MPa	
Graphite CL	408	+1393 ± 8		[a]
Graphite L	408	+1360 ± 5		[a]
Graphite F	408	+1078 ± 3		[a]
Glassy carbon	408	+18 ± 2		Solid deposition on surface
SiC	408	−51 ± 3		No corrosion observed
Stainless steel	408	−72 ± 3		Localized pitting corrosion
Alumina	408	−5144 ± 24		Strong intergranular corrosion: grain detachment
ZrO_2–Y_2O_3	<144	Disintegrated		
Graphite F	383		+1159 ± 3	[a]
Graphite L	383		+1021 ± 4	[a]
Graphite CL	383		+539 ± 4	[a]
Alumina	383		+240 ± 2	Slight intergranular corrosion
Graphite np	383		+240 ± 1	[a]
Stainless steel	383		+98 ± 2	Cavity formation: surface peeling.
Glassy carbon	383		+15 ± 2	Solid deposition on surface
SiC	383		−2201 ± 12	Dissolution, porous layer and crack formation

[a] Fluid intrusion and mineral formation into porosities.

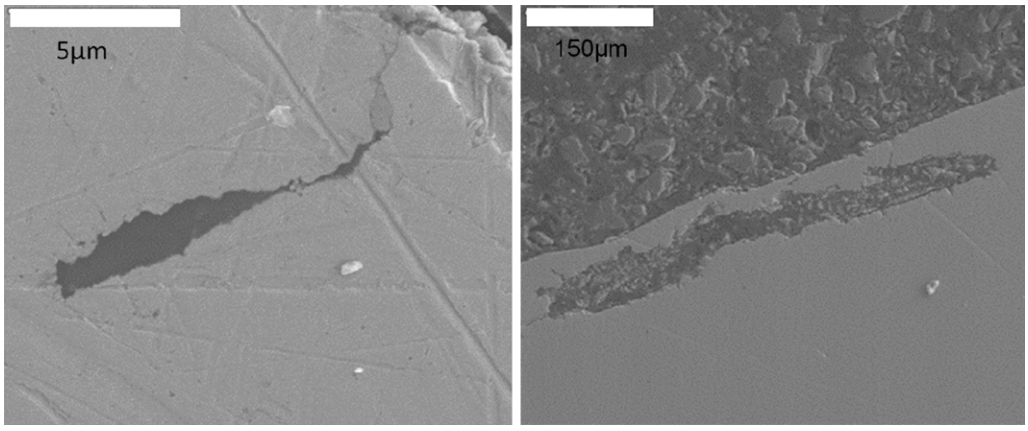

Fig. 4. (Left) Pitting corrosion on SS316 L surface in subcritical deionized water (335 °C, 21.5 MPa). (Right) Peeling of the SS316 L surface in supercritical water in the presence of vinasse (550 °C, 25.0 MPa). Similar peeling effect is observed in supercritical water and in subcritical water in the presence of vinasse.

Kritzer.[9] A 316 L stainless steel is used as a corrosion reference because it is supposed to be easily corroded in supercritical water and be used as a witness of the corrosive environment. Indeed, we also followed the evolution of our gasification reactor made of 718 Inconel®.

As can be seen in Fig. 3, the 316 L stainless steel does not show any mass loss, neither in water nor in water in the presence of biomass whatever the temperature and pressure conditions. However, corrosion is observed in every condition. In pure water, where the prevailing conditions are close to that of the critical point (330 °C and 21.5 MPa) one can observe a localized pitting corrosion. SEM observation shows pits with 5–10 µm length. This corrosion occurs locally, along grain boundary. In supercritical fluids (pure deionized water and vinasse) and in vinasse under subcritical conditions the material dissolution causes the formation of cavities where solutions can concentrate (Fig. 4). This phenomenon is reinforced in supercritical conditions by the formation of an oxidative front that may be attacked by active dissolution.[29] This explains the surface "skin" removal observed.

Inconel® 718 seems to be insensitive in pure water, only localized "pitting" corrosion is observed (not shown here). But in the presence of vinasse the same peeling effect is observed with a larger magnitude. Strong material loss occurred in the case of aqueous biomass at high temperature. After 5–10 days in the supercritical vinasse, the sample carrier was almost completely destroyed and a significant quantity of the reactor surface had been removed with the reaction product (Fig. 5). A SEM analysis of these particles shows that there is a preferential dissolution of the Cr and a precipitation of almost pure Ni particles.

3.2.2. Y-stabilized zirconia

In our experiments, zircon dioxide stabilized with Y_2O_3 was destroyed in less than 144 h (6 days) in subcritical water in the presence of vinasse (Table 7). It confirms the results obtained by Boukis et al.[21] on pure zirconia and on zirconia with different molar fraction of yttrium in SCWO conditions.

3.2.3. Alumina

Alumina has a constant mass loss in subcritical water conditions (Fig. 3a and c) both in deionized water and in concentrated vinasse. But the magnitude is more important in the presence of vinasse. In pure water, the mass loss is less than −0.5 wt.% of the initial mass while it reached −8 wt.% in the water containing organic matter. SEM analysis shows a strong intergranular corrosion when operating in the subcritical conditions (Fig. 6). In the presence of biomass, the association of Al with species available in the solution (Si, Ca, etc.) allows for the formation of solids (aluminosilicates). As a consequence the dissolution rates of alumina increase by equilibrium shift.

In supercritical water conditions at 550 °C and 25 MPa no significant weight change has been measured for alumina whatever the medium (Fig. 3d). However one can observe a slight intergranular corrosion (Fig. 7).

This material perfectly illustrates the well-known fact that subcritical conditions are more corrosive than supercritical ones. In the subcritical water, close to the critical point, the ionic product of water is higher than it is at ambient temperature. Most acids and salts follow the same trend because the water density and electric coefficient are still high enough to allow the hydration of

Fig. 5. Peeling effect on our batch reactor made of Inconel® 718.

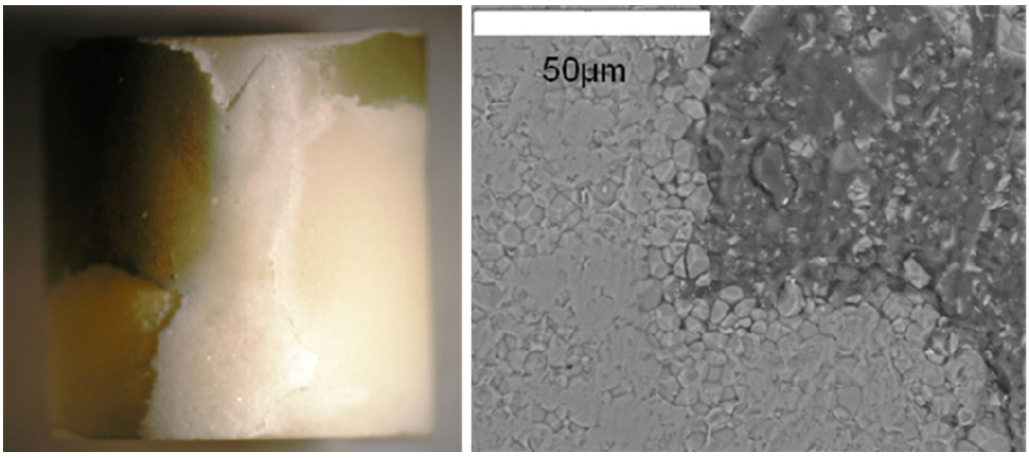

Fig. 6. (Left) Picture of the alumina sample after 120 h in subcritical water in the presence of vinasse (330 °C, 25.0 MPa). (Right) On the SEM images of the sample after 400 h we can see the strong intergranular corrosion leading to grain detachment from the surface.

ionic species. In these conditions water is an effective medium for acid or base reactions. On the contrary, in supercritical water, all these parameters (ionic product, density, dielectric constant) decrease drastically, so water becomes a poor medium for ionic reactions and ionic dissociation of simple salt and acids (NaCl and HCl) becomes very weak.[1,2,9]

3.2.4. SiC

Contrary to the alumina ceramic, the SiC ceramic exhibits a severe corrosion in the supercritical fluids (Fig. 8) whereas it was not observed in subcritical conditions (both in pure water and vinasse). The mass loss is significant in pure water and in vinasse in supercritical conditions (respectively 15 mg cm^{-2} (−2.5 wt.%) after approximately 400 h and 22 mg cm^{-2} (−4.6 wt.%) after 383 h of exposition) (Fig. 3).

In supercritical water, cristoballite crystals are formed on the face in contact with the sample carrier (Fig. 8). Its formation probably results from a poor exchange between the product of dissolution close to the surface and the fluid. The composition and the nature of these crystals have been determined by EDS and Raman spectroscopy.

Similarly when aqueous biomass is used, one can observe a porous SiO_2 cristoballite oxide layer that forms a crust on the unexposed face, in a manner similar to the one previously explained.

3.2.5. Graphite and glassy carbon materials

Several kinds of graphites have been characterized. X ray diffraction shows that each material has the same crystallographic hexagonal structure (2H). Glassy carbon is a vitreous carbon which exhibits a crystallographic disorder. It is designed as sheets with a maximal thickness of 3 mm. All graphite peaks are present on the X-ray diffractogram but with large bands. Actually, in this material the graphitic sheets are formed only on 2 or 3 layers.

The route to commercial graphites might differ depending upon the way they are elaborated and so does their macroscopic structure. For instance the porous volume varies from one graphite to another (Table 4), but also the pore size distribution that affects the surface to volume ratio. Hg-porosimetry on graphite F shows an open porosity of 18% (Table 4) with 2 peaks on the differential intrusion diagram at 15 µm and 0.012 µm. This diagram gives us the Hg quantity (mg l^{-1}) injected in the material as a function of the pore diameter. It shows a large pores distribution around the 2 main peaks. For graphite CL, the grain sizes are in the range 8–15 µm. The open porosity

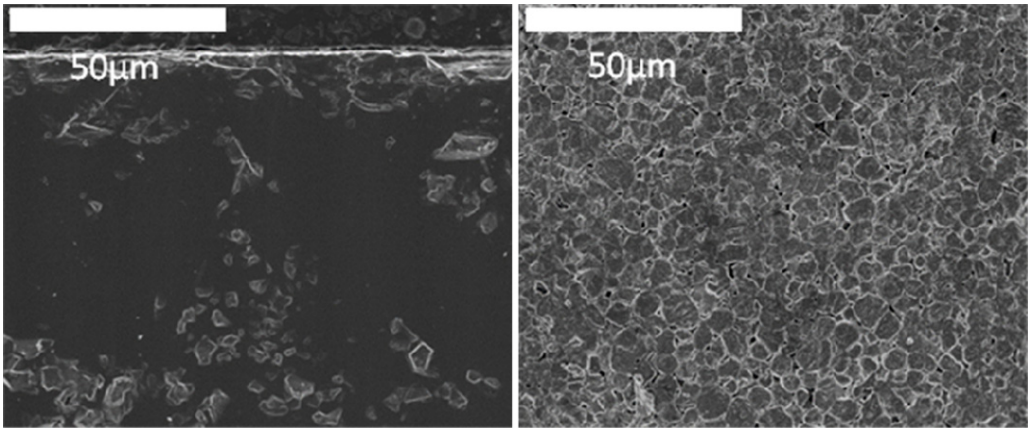

Fig. 7. Alumina surface before and after the chemical attack in supercritical water in the presence of vinasse (550 °C, 25.0 MPa).

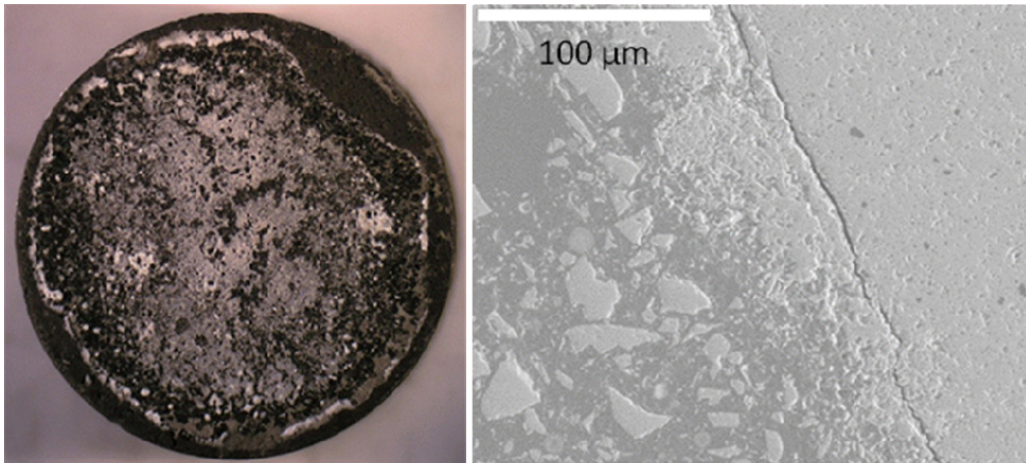

Fig. 8. On the left, picture of the SiC sample after contact with supercritical water in the presence of vinasse. The formation of a white cristoballite crust can be seen on the surface. On the right, SEM picture of the SiC in the pure supercritical water. The formation of a porous layer and cracks can be observed.

is 18% and there is a small pore distribution around 2.2 μm. Graphite L shows large pores on the surface and a huge poral volume of 33%. On the intrusion diagram there is only one peak at 3.6 μm. For glassy carbon the open porosity is nil, and only small nanometric closed porosity are present on the sample surface.

After 500 h in the subcritical deionized water (Fig. 3a) graphite F has a slight mass gain (+0.3 wt.%) similar to that measured on the non-porous graphite np (+0.3 wt.%) (with a residual porosity of 0.5%). The pressurized water fills the nanometric pores during the experiment and could not be removed by the drying protocol at 150 °C or in a primary vacuum (10^{-3} bar). Other graphite based materials do not show significant mass loss except for graphite L (where the mass loss reaches −0.3 wt.%). Graphite materials do not react significantly with subcritical water. But except glassy carbon, all graphic materials have a constant mass loss in deionized water at 550 °C and 25 MPa (Fig. 3b). The phenomenon is not negligible because this mass loss ranges from 1 to 5 wt.%. An oxidation reaction takes place in the first hours and then stops. This is the reason why the sample mass remains almost constant with time. Optical and electronic microscopic analysis does not allow for the observation of any changes in the material structure. Graphite F is less affected by this oxidation because of its structural characteristic. It has the same porosity as graphite CL but its specific surface is lower according to the presence of a pore distribution around 15 μm.

Magne et al.[30] give us a possible explanation of the observed mass loss. From 200 °C the water forms a complex with graphite that may decompose into CO and H_2 which increases with the temperature. No CO desorption occurs before 345 °C, so the graphite remains very stable in the subcritical aqueous solutions. The authors demonstrate the presence of 2 specific types of sites for water adsorption. The first kind of sites is formed by labile carbon atoms. These atoms are not well linked to the others and create a local disorder. The CO desorption becomes significant from 500 °C and stops when all the labile carbon atoms are removed. These specific sites are not renewable; this may explain our observations, i.e. a constant mass loss after a few hours in supercritical water at 550 °C and 25 MPa. The second kind of sites is made of atoms normally linked to the graphite lattice. They are constantly renewed after degassing CO molecules. For Magne et al.,[30] this reaction starts in the 738–806 °C temperature range. Temperatures around 800 °C may limit the use of graphite in pure water.

After approximately 400 h of exposure to biomass in water at 350 °C and 25 MPa, all porous graphites have a significant mass gain ranging from 2.7 to 5.8 wt.%. This is due to the fluid intrusion inside the materials under the pressure conditions during the experiment. A precipitation of white solids, mainly composed of potassium sodium and oxygen, is observed (Fig. 9). X-ray diffraction allows us to determine the presence of solid reaction products that belongs to the carbonate family (Na_2CO_3, K_2CO_3 and $KHCO_3$). Non-porous glassy carbon does not show significant mass variation (+0.1 wt.%).

When aqueous biomass is subjected to supercritical water conditions, a mass gain correlated to the formation of potassium-based solids is also observed (+1.7–4.5 wt.% within the same time conditions). The corrosion of graphite has not been observed with SEM images for two reasons. Firstly, it may be of low magnitude and secondly, it is probably hidden by surface defects (Fig. 10). It is difficult to ensure that no reaction occurs with water, but we expect the formation of reductive gases (H_2, CO, CH_4) during gasification to neutralize the water–graphite reaction. This protective effect will be efficient even at higher temperature. This argument will be developed in the following discussion.

4. Discussion

Raw materials roughness is variable and can be high because of porosity or grain size (see graphite or SiC 100 Table 4). In the present study no specific surface preparation has been made so we are not able to establish a correlation between roughness and corrosion. Main corrosion parameters are supposed to be chemical composition and mineralogy. Surface roughness may operate with less magnitude.

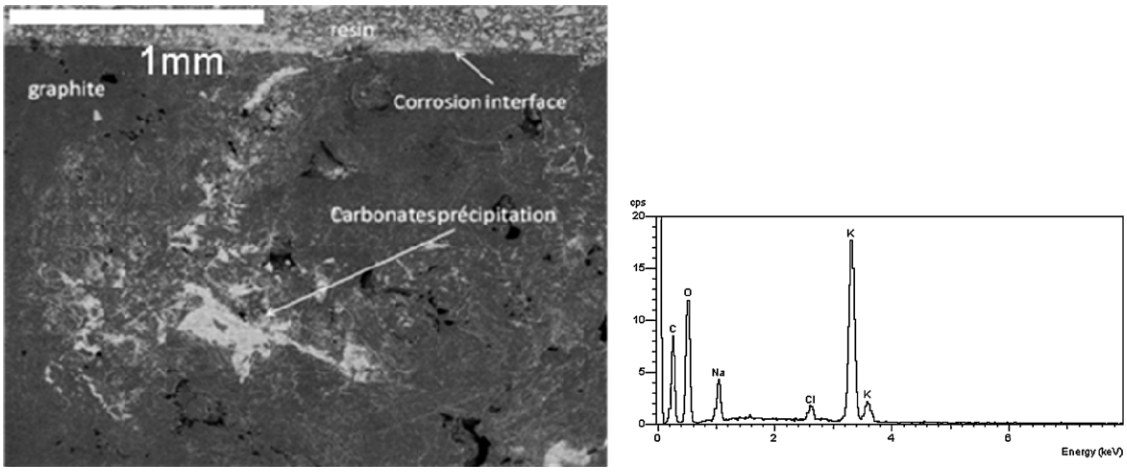

Fig. 9. On the left, SEM image of the precipitation of carbonates (K and Ca) and hydrogen carbonates ($KHCO_3$) in the graphite porosity after 400 h in vinasse at 350 °C and 25.0 MPa. On the right, EDX spectra of the carbonates.

4.1. Corrosion of Si and SiO_2 based material

Hydrothermal corrosion of SiC and Si_3N_4 leads to the formation of SiO_2, CH_4 and NH_3. Global reactions are:[31]

$$Si_3N_4 + 6H_2O = 3SiO_2 + 4NH_3 \quad (1)$$

$$SiC + 2H_2O = SiO_2 + CH_4 \quad (2)$$

As a consequence, silicon nitride ceramic is strongly altered in sub- and supercritical conditions.[27,32] Boukis et al.[21] confirmed this behavior for SiC, Si_3N_4 and SiAlON. According to our observations the nitrogen gasification is faster than the silica (SiO_2) dissolution and a great depletion in N atoms is thus measured in the Si_3N_4. Si_3N_4 and BN disintegrate whereas AlN is covered with a thick alumina layer.[21] SiC material corrosion in deoxygenated water seems to occur at a very low rate, but this rate may increase drastically changing the pH.[22] In supercritical water at 500 °C, the corrosion takes place at grain boundaries.[22] We observe the same mechanisms on SiC 100; this sample has a large grain size and a high porosity (Table 2). In subcritical water at 300 °C and 10 MPa Henager et al.[33] observed a pitting corrosion after 4000 h of exposure. In our conditions, the exposure time range is 300–500 h which could explain the absence of corrosion during the subcritical water treatment in pure water and in the presence of vinasse.

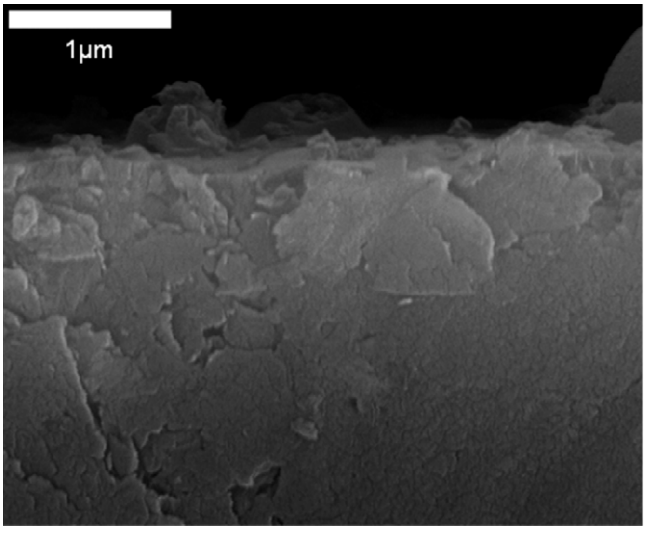

Fig. 10. SEM image of dense graphite after 15 days in supercritical water in the presence of vinasse (550 °C and 25.0 MPa). The corrosion cannot be distinguished from the surface defect and may occur at a lower scale (under 1 µm). The small cracks on the surface are due to the gold particles deposited on the surface for electron conduction.

Basically in the presence of O_2, the Si contained in ceramics acts as a protective layer in oxidizing environment thanks to the formation of a non porous SiO_2 layer that prevents O_2 diffusion. In the presence of water the solubility of SiO_2 at high temperature does not allow the formation of this stable protective layer. Corrosion of SiO_2 based material acts in two steps, the first one is the formation of the SiO_2 layer and the second one is the dissolution of this layer. As discussed by Kritzer in[9] the solubility of oxides plays a key role in corrosion phenomenon. Indeed, all can be summed up here as the study of silicon oxides dissolution in water.

From the experimental point of view, SiO_2 based materials (aluminosilicate, cordierite-mullite) are highly corroded in hydrothermal conditions. The dissolution of silica at high temperature and high pressure, from the subcritical to the supercritical water has been well studied.[34–36] To reach the supercritical water conditions in batch experiments, one follows the water pressure saturation curve from the ambient conditions up to the critical point of water. In the subcritical water conditions (diphasic domain), materials can be first exposed to liquid water and to the water vapor. It is known that water vapor plays an important role in silica volatilization:[37]

$$SiO_2(s) + 2H_2O(g) = Si(OH)_4(g). \quad (3)$$

This phenomenon increases as a function of water vapor partial pressure and keeps on increasing up to the critical point. In supercritical water, silica dissolves into monosilicic acid $Si(OH)_4$.[38] Even if silica solubility in low pressure supercritical water is less than in high density SCW, at elevated

temperature the silica dissolution reaction reaches its equilibrium faster. In addition, the presence of salt, like NaCl, increases the silica dissolution and its rate.[38,39] Models for predicting quartz solubility show that "the natural logarithm of the molality of dissolved silica ($\ln m_{SiO_2 \cdot nH_2O}$, with n = the hydration number), in equilibrium with quartz, is a function of the natural logarithm of the density of the solution ($\ln \rho$).[39] In biomass, different salts may be present in variable quantities (K_2SO_4, NaCl, KCl, $CaSO_4$, $CaCO_3$, etc.). Their presence may shift the silica dissolution equilibrium point by the formation of Si based minerals. The material corrosion is then increased by these additional reactions. The nature of the SiO_2 layer formed on the material surface is of great importance. Quartz crystal dissolution is slower than amorphous silica dissolution. Sõmiya[31] explains the SiC and Si_3N_4 reactions by the formation of an amorphous silica layer that is more consistent with the observations. Barringer et al.[22] believed that corrosion of the high purity SiC occurred via hydrolysis to hydrated silica species on the surface that were rapidly dissolved into the supercritical water. In our work, in the supercritical water conditions, the formation of a cristoballite surface layer that could have been crystallized after SiO_2 solubility and precipitation is observed. The result is a concentration of dissolved species ($Si(OH)_4$) that must be in equilibrium with solid oxides forms (here cristoballite).

To summarize, all Si and silica based material even SiC are corroded by hot pressurized water (subcritical and supercritical water) and the corrosion becomes greater in the presence of biomass containing salts.

4.2. Corrosion of alumina and zirconia

Alumina is used in the SCWO process for the conversion of halogenated hydrocarbon.[26] This material is commonly used in the high temperature processes and in extreme environments. Boukis et al.[21] shows that pure alumina and alumina-based materials are stable in supercritical water, they note that only a slight general corrosion and no mass loss after 220 h at 465 °C were observed. In our experiments, this behavior in the supercritical fluids is confirmed but we found that subcritical water corrosion increased in the presence of vinasse. Alumina may be sensitive to acids depending on its nature, its concentration and the temperature. Schacht et al.[24] show that with a 0.1 mol kg^{-1} acid concentration, alumina is corroded. With HCl, the corrosion occurs only in the subcritical water solutions. With H_2SO_4 the corrosion reaches a maximum around 350 °C and becomes negligible only at 500 °C. No corrosion effects is detected with H_3PO_4, this is explained by the formation of a stable berlinite ($AlPO_4$) phase. Genthe et al.[40] show some different effects with the same acids. In their works the corrosion of alumina is more important in H_3PO_4, HCl and then H_2SO_4. This outlined the importance of the concentration of acids.

The dissolution of the yttrium stabilizing agent present inside the zirconia can lead to the degradation of the ceramic as a result of phase transition.[41,42] This transition from tetragonal toward monoclinic zircon causes a 5–6% volume expansion that has been identified as a cause of material cracking.[25] Yoshimura et al.[43] propose that, in hydrothermal conditions, water is adsorbed on the surface of the ceramic. Then hydroxides groups migrate through oxygen vacancies leading to the formation of zirconium and yttrium hydroxides. The stressed site defects at the oxygen vacancies acts as a site for the nucleation of the monoclinic phase. The mechanism of this hydrothermal degradation is not well understood and the role of water might be complex. But, it is confirmed that these materials are not relevant for the SCW process.

4.3. Corrosion of carbon material

The only studies devoted to graphite in supercritical water were made for nuclear applications. Indeed, graphite is an excellent moderator used in supercritical water-cooled reactors.[44] Unfortunately, nuclear radiations play a key role in materials corrosion. The gasification of graphite has been widely studied in the presence of air or oxygen. Few papers are devoted to the water–graphite interaction and to its gasification.[30] Graphite is resistant to oxidation in air at temperatures up to 400–500 °C.[45] But hydrothermal oxidation of graphite (mechanism and chemical equilibrium) is very different from oxidation in air. If graphite is put into contact with one atmosphere of helium saturated with water vapor at ambient temperature, then, at the atmospheric pressure and at variable temperatures the chemisorption of water on graphite becomes appreciable above 200 °C. In contact with water vapor, labile carbon atoms react with chemisorbed water to form CO and H_2.[30] This oxidation starts around 350 °C but is significant around 500 °C. When these carbon atoms, which can be considered as surface defect, are removed, no reaction is detected up to 800 °C. So the lethal condition for graphite in the presence of water seems to be around 800 °C at atmospheric pressure. It is far from our present working temperature conditions limited to 550 °C and also from our pressure conditions (25 MPa). As pressure has a lower effect on material reactivity than temperature, we expect that graphite materials are able to sustain oxidation in the presence of water up to 800 °C.

In this experimental work, it is shown that carbon materials are high performance materials for SCBG and that they may be used to protect or build reactors. The future of SCBG is clearly linked to our capability to design high temperature (550 °C < T < 800 °C) and high pressure (P = 25 MPa) reactors. Indeed, high temperature (800 °C) must be reached if we want to increase H_2 yield in SCWG[5,10,46] and increase carbon efficiency, define as the "degree of conversion of carbon in the biomass to permanent gases".[46,47] The carbon efficiency is a way to measure the rate of biomass gasification. This is especially true if concentrated organic biomass is used. A better knowledge of graphite gasification in water with biomass at temperature higher than 550 °C at 25 MPa is then of importance.

A second point of importance is the formation of gases from biomass gasification that create reductive conditions and may avoid graphite oxidation. There is no experimental apparatus that could allow us to determine the carbon material lifetime in such extreme conditions (T > 550 °C and P = 25 MPa) in the presence of biomass. The thermodynamical study of graphite oxidation was used to study the graphite stability in

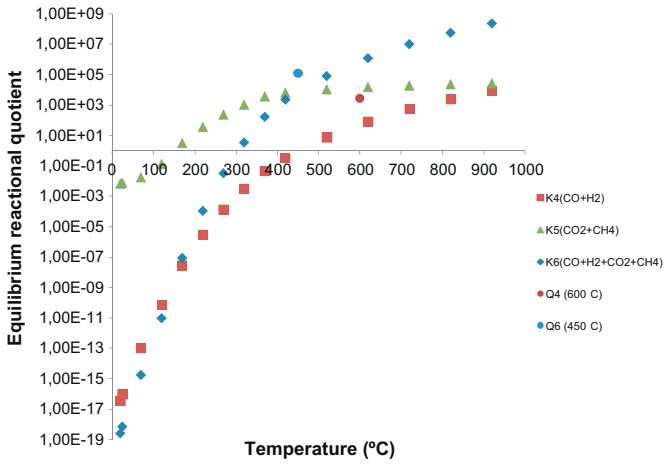

Fig. 11. Equilibrium coefficient K4 (T,P), K5 (T,P) and K6 (T,P) of the reactions, (4) $C + H_2O = CO + H_2$, (5) $2C + 2H_2O = CO_2 + CH_4$ and (6) = (4) + (5), K6 = K4 × K5. Q_i are the respective reaction quotients calculated with the theoretical gas composition in the continuous flow reactor. The (T,P) conditions follow the water vapor saturation curve up to the critical point of water (T_c = 374 °C). In the supercritical domain, the pressure is constant and P = 25.1 MPa.

oxygen-free supercritical water gasification processes, from ambient to supercritical water conditions (920 °C and 25 MPa).

4.4. Thermodynamical modelling

The water–graphite reaction was studied with a thermodynamical modelling from ambient conditions up to 920 °C. In these conditions, the graphite may be involved in three oxidation reactions:

$$C + H_2O = CO + H_2 \quad (4)$$

$$2C + 2H_2O = CO_2 + CH_4 \quad (5)$$

$$3C + 3H_2O = CO + H_2 + CO_2 + CH_4 \quad (6)$$

We studied each reaction and the evolution of their equilibrium reactional quotient with temperature (Fig. 11). To fit with our batch conditions, the (T,P) conditions are determined by the liquid/vapor saturation curve of water up to the critical point. In the supercritical domain of water the pressure is constant and P = 25.1 MPa.

The SUPCRT92 software[48] is well suited for the study of reactions in supercritical water. It allows us to calculate the thermodynamic properties of the balanced chemical reaction from 1 to 500 MPa and 0 to 1000 °C. Using SUPCRT92, apparent standard molal Gibbs free energies of the reactions are calculated. Apparent energies are defined at any T and P according to the following formulation recalled by Johnson et al.[48]:

$$\Delta G^\circ_{P,T} = \Delta G^\circ_f + (G^\circ_{P,T} - G^\circ_{P_r,T_r}) \quad (7)$$

ΔG°_f denotes the standard molal Gibbs free energy of formation of the species from its elements in stable phase at the reference pressure (P_r = 1 bar) and temperature (T_r = 298.15 K). ($G^\circ_{P,T} - G^\circ_{P_r,T_r}$) refers to the difference in the standard molal Gibbs free energy that arises from changes in the pressure ($P - P_r$) and temperature ($T - T_r$).

From this definition one can define K (T,P) by the classical relation:

$$\Delta G^\circ_{P,T} = -RT \ln K(T, P) \quad (8)$$

The evolution of the graphite–water equilibrium in the environment created by the biomass gasification in the continuous flow reactor was also studied. A mathematical model for supercritical water gasification of vinasse, based on thermodynamical equilibrium assumption, has been built.[49,50] Gas composition, fugacity coefficients and activities of the chemical species, including CO, H_2, CO_2, CH_4 and H_2O were estimated using Peng–Robinson equation of state. A theoretical gas composition in the reactor was obtained at equilibrium and at T = 450 °C and 600 °C. To study the thermodynamical stability of graphite in the presence of the gas resulting from supercritical water gasification of vinasse; we deduced from this composition a theoretical reactional quotient (Q_i) for the graphite oxidation reaction (i). The gas composition calculated is at equilibrium for the vinasse gasification reaction but is probably not in equilibrium according to the graphite oxidation reactions. The quotient Q_i is defined as the activities quotient of reactant and product involved in the graphite oxidation reaction (i). Q_i at 450 °C and 600 °C were calculated respectively for reactions (6) and (4) and compared to the equilibrium coefficient K_i (T,P) (Fig. 11). The Q_i coefficients are always greater than their respective equilibrium coefficient K_i. It means that the graphite oxidation reactions are likely to occur in the direction of graphite formation:

$$\Delta G_r = RT \ln \frac{Q}{K} > 0. \quad (9)$$

In other words, graphite is stable because a reductive atmosphere is formed by biomass gasification.

5. Conclusion

Many ceramics are not suitable in hydrothermal environments and cannot sustain corrosion in our working conditions. The contact of hot pressurized water with or without vinasse leads to a significant mass loss for most of ceramics into few hours. SiC is unable to sustain supercritical water conditions whereas alumina is corroded in subcritical water conditions. However, we indentified graphite and glassy carbon as candidate materials to build SCWG reactors.

These materials are interesting for two reasons: (1) their chemical reactivity is low and the presence of a reductive atmosphere promotes their chemical stability. Thus, this material may solve the corrosion problem and may be used to build reactors that could gasify many different feedstock and (2) they could also be used at higher temperatures up to 800 °C, thus allowing a technological leap, with increasing hydrogen yield and carbon efficiency without any need for catalysts.

In the present paper we defined the corrosion resistance of carbon materials on purely chemical arguments without addressing the question of their mechanical stability Many solutions are possible to solve the problem of mechanical stability, basically

we have to ensure the equipressure inside and outside the reactor or reinforce its capability to sustain mechanical stress. A SCBG reactor working up to 800 °C at 25 MPa is under construction using carbon materials. Its design is based on innovative solutions that will be presented in a further publication dealing with SCBG at high temperature.

Acknowledgments

The authors thank ANR (AgenceNational de la Recherche, France) and the PNRB (Programme National de Recherche sur les Bioenergies) for their helpful financial contribution in this research. We also thank the UNGDA (Union National du Groupement des Distillateurs d'Alcool) for his technical support.

References

1. Loppinet-Serani A, Aymonier C, Cansell F. Current and foreseeable applications of supercritical water for energy and the environment. *ChemSusChem* 2008;**1**:486–503.
2. Loppinet-Serani A, Aymonier C, Cansell F. Supercritical water for environmental technologies. *J Chem Technol Biotechnol* 2010;**85**:583–9.
3. Aymonier C, Lopinet-Serani A, Reveron H, Garrabos Y, Cansell F. Review of supercritical fluids in inorganic materials science. *J Supercrit Fluids* 2006;**38**:242–51.
4. Guo LJ, Lu YJ, Zhang XM, Ji CM, Guan Y, Pei AX. Hydrogen production by biomass gasification in supercritical water: a systematic experimental and analytical study. *Catal today* 2007;**129**:275–86.
5. Kruse A. Supercritical water gasification. *Biofuels Bioprod Biorefining* 2008;**2**:415–37.
6. Carrier M, Loppinet-Serani A, Absalon C, Marias F, Aymonier C, Mench M. Conversion of fern (*Pteris vittata* L.) biomass from a phytoremediation trial in sub- and supercritical water conditions. *Biomass Bioenerg* 2011;**35**:872–83.
7. Bühler W, Dinjus E, Ederer HJ, Kruse A, Mas C. Ionic reactions and pyrolysis of glycerol as competing reaction pathways in near- and supercritical water. *J Supercrit Fluids* 2002;**22**:37–53.
8. Zhang Y, Zhang J, Zhao L, Sheng C. Decomposition of formic acid in supercritical water. *Energ Fuels* 2010;**24**:95–9.
9. Kritzer P. Corrosion in high-temperature and supercritical water and aqueous solutions: a review. *J Supercrit Fluids* 2004;**29**:1–29.
10. Kruse A. Hydrothermal biomass gasification. *J Supercrit Fluids* 2009;**47**:391–9.
11. Marrone PA, Hong GT. Corrosion control methods in supercritical water oxidation and gasification processes. *J Supercrit Fluids* 2009;**51**:83–103.
12. Kritzer P, Boukis N, Dinjus E. The corrosion of alloy 625 (NiCr22Mo9Nb; 2.4856) in high-temperature, high pressure aqueous solutions of phosphoric acid and oxygen. Corrosion at sub- and supercritical temperatures. *Mater Corros* 1998;**49**:831–9.
13. Kritzer P, Boukis N, Dinjus E. The corrosion of nickel-base alloy 625 in sub- and supercritical aqueous solutions of oxygen: a long time study. *J Mater Sci Lett* 1999;**18**:1845–7.
14. Kritzer P, Boukis N, Dinjus E. Factors controlling corrosion in high-temperature aqueous solutions: a contribution to the dissociation and solubility data influencing corrosion processes. *J Supercrit Fluids* 1999;**15**:205–27.
15. Kritzer P, Boukis N, Dinjus E. The corrosion of nickel-based alloys 625 in sub- and supercritical aqueous solutions of HNO_3 in the presence of oxygen. *J Mater Sci Lett* 1999;**18**:771–3.
16. Mitton DB, Yoon J-H, Cline JA, Kim H-S, Eliaz N, Latanision RM. Corrosion behaviour of nickel-based alloys in supercritical water oxidation systems. *Ind Eng Chem Res* 2000;**39**:4689–96.
17. Hwang SH, Lee BH, Kim JG, Jang J. SCC and corrosion evaluations of the F/M steels for a supercritical water reactor. *J Nucl Mater* 2008;**372**:177–81.
18. D'Jesus P, Boukis N, Kraushaar-Czarnetzki B, Dinjus E. Influence of process variables on gasification of corn silage in supercritical water. *Ind Eng Chem Res* 2006;**45**:1622–30.
19. Calzavara Y, Joussot-Dubien C, Boissonnet G, Sarrade S. Evaluation of biomass gasification in supercritical water process for hydrogen production. *Energ Convers Manage* 2005;**46**:615–31.
20. Schmieder H, Abeln J. Supercritical water oxidation: state of the art. *Chem Eng Technol* 1999;**22**:903–8.
21. Boukis N, Claussen N, Ebert K, Janssen R, Schacht M. Corrosion screening test of high performance ceramics in supercritical water containing oxygen and hydrochloric acid. *J Eur Ceram Soc* 1997;**17**:71–6.
22. Barringer E, Faiztompkins Z, Feinroth H. Corrosion of CVD silicon carbide in 500 °C supercritical water. *J Am Ceram Soc* 2007;**90**:315–8.
23. Tan L, Allen TR, Barringer E. Effect of microstructure on the corrosion of CVD-SiC exposed to supercritical water. *J Nucl Mater* 2009;**394**:95–101.
24. Schacht M, Boukis N, Dinjus E. Corrosion of alumina ceramics in acidic aqueous solutions at high temperatures and pressures. *J Mater Sci* 2000;**35**:6251–8.
25. Schacht M, Boukis N, Dinjus E, Ebert K, Janssen R, Meschke F, et al. Corrosion of zirconia ceramics in acidic solutions at high pressures and temperatures. *J Eur Ceram Soc* 1998;**18**:2373–6.
26. Lee H-C, In J-H, Lee S-Y, Kim J-H, Lee C-H. An anti-corrosive reactor for the decomposition of halogenated hydrocarbons with supercritical water oxidation. *J Supercrit Fluids* 2005;**36**:59–69.
27. Proverbio E, Carassiti F. Low-temperature oxidation of silicon nitride by water in supercritical condition. *J Eur Ceram Soc* 1996;**16**:1121–6.
28. Escot Bocanegra P, Reverte C, Aymonier C, Loppinet-Serani A, Barsan MM, Butler IS, et al. Gasification study of winery waste using a hydrothermal diamond anvil cell. *J Supercrit Fluids* 2009;**53**:72–81.
29. Ampornrat P, Was GS. Oxidation of ferritic–martensitic alloys T91, HCM12A and HT-9 in supercritical water. *J Nucl Mater* 2007;**371**:1–17.
30. Magne P, Sauvageot R, Duval X. Etude de la formation d'un complexe de surface graphite-eau. Relation avec la réaction d'oxydation. *Carbon* 1973;**11**:485–95.
31. Sõmiya S. Hydrothermal corrosion of nitride and carbide of silicon. *Mater Chem Phys* 2001;**67**:157–64.
32. Sato T, Murakami T, Endo T, Shimada M. Corrosion of silicon nitride ceramics under hydrothermal conditions. *J Mater Sci* 1991;**26**:1749–54.
33. Henager Jr CH, Schemer-Kohrn AL, Pitman SG, Senor DJ, Geelhood KJ, Painter CL. Pitting corrosion in CVD SiC at 300 °C in deoxygenated high-purity water. *J Nucl Mater* 2008;**378**:9–16.
34. Anderson GM, Burnham CW. The solubility of quartz in supercritical water. *Am J Sci* 1965;**263**:494–511.
35. Fournier RO, Rowe JJ. The solubility of amorphous silica in water at high temperatures and high pressures. *Am Miner* 1977;**62**:1052–6.
36. Shin HY, Matsumoto K, Higashi H, Iwai Y, Arai Y. Development of a solution model to correlate solubilities of inorganic compounds in water vapour under high temperatures and pressures. *J Supercrit Fluids* 2001;**21**:105–10.
37. Jacobson NS, Opila EJ, Lee KN. Oxidation and corrosion of ceramics and ceramic matrix composites. *Curr Opin Solid State Mater Sci* 2001;**5**:301–9.
38. Kitahara S. The solubility equilibrium and the rate of solution of quartz in water at high temperatures and high pressures. *Rev Phys Chem Jpn* 1960;**30**:122–30.
39. Von Damm KL, Bischoff JL, Rosenbauer RJ. Quartz solubility in hydrothermal seawater: an experimental study and equation describing quartz solubility for up to 0.5 M NaCl solutions. *Am J Sci* 1991;**291**:977–1007.
40. Genthe W, Hausner H. Influence of chemical composition on corrosion of alumina in acids and caustic solutions. *J Eur Ceram Soc* 1992;**9**:417.
41. Lange F, Dunlop G, Davis B. Degradation during aging of transformation-toughened ZrO_2–Y_2O_3 materials at 250 °C. *J Am Ceram Soc* 1986;**69**:237–40.
42. Kimel RA, Adair JH. Aqueous degradation and chemical passivation of yttria-tetragonally-stabilized zirconia at 25 °C. *J Am Ceram Soc* 2002;**85**:1403–8.
43. Yoshimura M, Noma T, Kawabata K, Somiya S. Role of H_2O on the degradation process of Y-TZP. *J Mater Sci Lett* 1987;**6**:465–7.

44. Abram T, Ion S. Generation-IV nuclear power: a review of the state of the science. *Energ Policy* 2008;**36**:4323–30.
45. Xiaowei L, Jean-Charles R, Suyuan Y. Effect of temperature on graphite oxidation behavior. *Nucl Eng Des* 2004;**227**:273–80.
46. Matsumura Y, Minowa T, Potic B, Kersten SRA, Prins W, van Swaaij WPM, et al. Biomass gasification in near- and super-critical water: status and prospects. *Biomass Bioenerg* 2005;**29**:269–92.
47. Potic B, Kersten SRA, Prins W, van Swaaij WPM. A high throughput screening technique for conversion in hot compressed water. *Ind Eng Chem Res* 2004;**43**:4580–4.
48. Johnson JW, Oelkers EH, Helgeson HC. SUPCRT92: a software package for calculating the standard molal thermodynamic properties of minerals, gases, aqueous species and reactions from 1 to 5000 bars and 0 to 1000 °C. *Comput Geosci* 1992;**18**:899–947.
49. Letellier S, Marias F, Cezac P, Serin JP. Gasification of aqueous biomass in supercritical water: a thermodynamic equilibrium analysis. *J Supercrit Fluids* 2010;**51**:353–61.
50. Marias F, Letellier S, Cezac P, Serin JP. Energetic analysis of gasification of aqueous biomass in supercritical water. *Biomass Bioenerg* 2011;**35**:59–73.